
Article:
Liu, X. orcid.org/0000-0003-2419-2214, Zhou, H. orcid.org/0000-0002-6806-1366, Lai, Y. orcid.org/0000-0002-9987-0975 et al. (1 more author) (2023) Equivalence ratio independence and dependence ranges of system responses for a nonlinear thermoacoustic oscillation in a Rijke tube. Journal of Sound and Vibration, 547. 117545. ISSN 0022-460X

https://doi.org/10.1016/j.jsv.2022.117545

Journal of Sound and Vibration 547 (2023) 117545

Contents lists available at ScienceDirect

Journal of Sound and Vibration

journal homepage: www.elsevier.com/locate/jsvi

Equivalence ratio independence and dependence ranges of system responses for a nonlinear thermoacoustic oscillation in a Rijke tube

Xuanqi Liu [a], Hangxu Zhou [a], Yufeng Lai [b], Yang Zhang [a,*]

[a] Department of Mechanical Engineering, The University of Sheffield, Sheffield S1 3JD, UK
[b] Department of Electronic and Electrical Engineering, The University of Sheffield, Sheffield S1 3JD, UK

ARTICLE INFO

Keywords:
Thermoacoustics
Rijke tube
Nonlinear system
Time-domain analysis
Recurrence analysis

ABSTRACT

Thermoacoustic instabilities in a combustion system remains a challengeable problem in industry over decades. It usually involves with the nonlinear interaction between unsteady heat release and pressure fluctuations. The nonlinear oscillation excited by this interaction can be intense enough to result in combustion problems even severe damage of the engine. Therefore, it is important to understand the system response to various parameters. In this study, the system nonlinearity to equivalence ratio change was mainly focused on. A Rijke tube system with a premixed methane-air laminar flame was utilised to trigger the self-excited oscillations with varied equivalence ratios (Φ). The time-domain analysis methods including phase difference, Recurrence Plot (RP) and Recurrence quantification analysis (RQA) were applied to obtain the characteristics of system nonlinearities. Both Φ-independence and Φ-dependence ranges of system frequency responses have been discovered. The results of phase difference and recurrence analysis have also validated the finding of both ranges. The corresponding characteristics of system nonlinearity in both ranges have been investigated. The similarity among the systems in the Φ-independence range under the same burner position and methane flowrate can be highlighted from the system frequency response, phase difference and system dynamics. It is found that the phase difference analysis, RP and RQA utilised in this study are capable of investigating the nonlinearities of the self-excited thermoacoustic oscillation.

1. Introduction

Thermoacoustic instability has been one of the most challenging yet unignorable problems during the development of gas turbines for decades. The self-excited oscillation caused by the instability is highly possibly triggered in an acoustic resonator which involves combustion or heat exchanges [1–3]. Rayleigh revealed the mechanism of triggering thermoacoustic oscillation, that is the coupling effect between unsteady heat release rate and pressure fluctuations when they are in-phase [4], which is known as the Rayleigh Criterion. However, as a qualitative description, Rayleigh Criterion is hard to obtain information about the stability of the system and quantify the system behaviour.

Although successful theoretical models have been built for revealing the excitation mechanism of thermoacoustic instabilities [1,

* Corresponding author.
E-mail address: yz100@sheffield.ac.uk (Y. Zhang).

https://doi.org/10.1016/j.jsv.2022.117545
Received 4 August 2022; Received in revised form 20 December 2022; Accepted 27 December 2022
Available online 28 December 2022

5–9], the insightful information for identifying the system dynamics in a combustion system remains insufficient. Aiming at investigating the nonlinear thermoacoustic oscillation, the Rijke tube has been widely used to conduct experimental studies in a laboratory scale [10–16]. It has been found that the combustion-induced thermoacoustic instabilities in a Rijke tube are mainly attributed to complex nonlinear interaction among acoustic, flame properties and hydrodynamics [17]. The nonlinear relationships between the interactions and system responses have been extensively focused on [3,11,17–20, 13]. For instance, the oscillation amplitude and system frequency response can be affected by airflow around the flame and nozzle position to different extents [15]. Zhang et al. noted the importance of fuel supply flow and swirl number on the oscillation in lean combustion with a swirl burner [21]. Heckl and Howe studied the effects of the hydrodynamic region on the self-excited oscillation in a Rijke tube with a flame holder [19]. A nonlinear mathematic model was proposed to explain the influence of hydrodynamic range on both system frequency response and oscillation amplitude. Zhao and Chow further developed the hydrodynamic region theory by introducing the drag effect of ambient fluid after the experimental investigations in a Rijke tube [11]. Many experimental studies have been conducted to indicate the crucial role of equivalence ratios in thermoacoustic instabilities, such as the critical condition for triggering a self-excited sounding [22], possible equivalence ratio ranges for triggering beating oscillations [16], and trends of eigenfrequencies and oscillation amplitude with varied equivalence ratios [23]. Besides, many numerical studies have been carried out to explain and predict thermoacoustic oscillation in various combustion systems. It has been proved in various combustors that the LES can successfully predict both the system eigenfrequency and the oscillation amplitude [24–26]. Based on the unsteady compressible Navier Stokes equation, good agreement between the numerical and experimental result of the mode frequency, mode shapes and oscillation amplitude were obtained in both the classic Rijke tube and Rijke-Zhao (Y-shape) tube [12,27]. It has also been found that numerical methods can be efficient for investigating quasi-periodic oscillation. Both the beating frequency and heat release fluctuation can be obtained from the numerical investigations [16,28].

The nonlinear thermoacoustic oscillation in a combustion system is caused by the complex interactions among several physical properties, which leads to the significantly time-varied system states. Therefore, the time domain statistical analysis and measurements can provide insightful and meaningful information to characterise the thermoacoustic system. Some studies applied two-microphone and multi-microphone techniques to investigate the acoustic-related properties (e.g. acoustic impedance, wave velocity and frequency composition) in a tube chamber with either self-excited oscillation or external acoustic source [29–32]. The phase space constructed based on the time-delay embedding method is extensively utilised to determine system intermittency and chaos-order transition in various combustion systems [17,33–35]. The recurrence analysis for the investigation of the thermoacoustic system was introduced, and great efforts were made by Sujith and Gotoda [35–41]. It has been found that the Recurrence plot (RP) can effectively describe and analyse combustion and thermoacoustic instabilities in various combustion systems [23,33,35–45]. The periodicity, chaoticity, state transition and intermittency can be indicated through the specific internal structure, pattern equality and density of recurrence points [23,33,35,44]. By applying the recurrence quantification analysis (RQA), the RP also can be used to identify system dynamics quantitatively [46]. As an effective analysis method, RP can efficiently identify the nonlinear relationship between system dynamics and system parameters.

Although many studies have investigated both the frequency response and oscillation amplitude under different system parameters, the studies for investigating the nonlinear trend of system eigenfrequency to equivalence ratio remain insufficient. Meanwhile, it has been reported the existence of internal nonlinear interaction between different harmonic modes in thermoacoustic oscillations [47]. Thus, the relative 'phase difference' between different modes can be important for indicating the characteristics of changes in time-evolution of pressure fluctuations. The thermoacoustic instabilities under fuel-rich conditions are also less studied, while fuel-rich combustion is more preferred in the field that requires higher combustion stability [48,49]. For example, the primary zone of Rich-burn, Quick-mix, Lean-burn (RQL) combustor dominates and initiates the combustion process. The equivalence ratio in the primary zone can be up to 2.5 [48]. Therefore, this work aims to intensively investigate the influence of the equivalence ratio on system

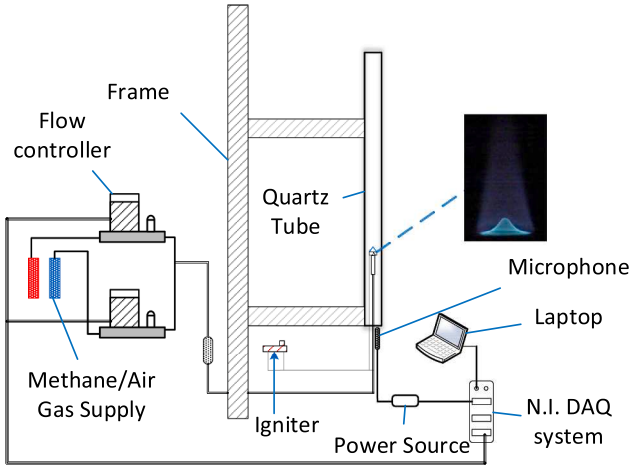

Fig. 1. Schematic figure of the flame-driven Rijke tube system.

nonlinearities in a Rijke tube. In this work, the eigenfrequency of self-excited oscillation, the phase difference between harmonic modes and system dynamics have been focused on. The pressure time series data of self-excited thermoacoustic oscillations under different conditions have been obtained in a Rijke tube with a laminar premixed flame. The time-domain analysis has been conducted to investigate the effect of the equivalence ratio on the phase difference and system dynamics properties through the phase differences and recurrence analysis. The phase difference between the harmonic modes was achieved by decomposing the pressure signal based on the FIR (Finite impulse response) phase-linear filter. The system dynamics were investigated and quantified by the recurrence plots (RP) and recurrence quantification analysis (RQA).

2. Experiment setup and data analysis method

2.1. Experimental setup

A vertically anchored Rijke tube was utilised to investigate the self-excited oscillations, with a heat source in the form of a laminar premixed methane flame. Fig. 1 shows the schematic figure of the experiment setup. The quartz tube of 1 m in total length was utilised in this study. A honeycomb flame holder of 28 mm in diameter was attached at the top of the nozzle for generating a stable conical shape premixed flame. The blockage ratio of the flame holder was about 22%. Since it has been reported that the effect of the flame holder on the thermoacoustic oscillations frequency can be neglected when the blockage ratio is smaller than 25% if the inlet Mach number is below 0.15 [1]. The flame was ignited by a single spark generated by a piezo spark igniter.

Aalborg GFC17 mass flow controllers were applied to control both air and methane flowrates with an accuracy of 0.05% for methane and 0.1% for air. The methane flowrates ($\dot{m}_{CH_4}$) were set as 0.65 L/min, 0.8 L/min and 0.95 L/min. Under a specific $\dot{m}_{CH_4}$, the equivalence ratio (Φ) ranged from 0.8 to 5.0, which is obtained by changing the air flowrate. It should be noted that those cases with too small equivalence ratios to trigger the oscillations were ignored in this study since this study mainly focuses on fuel-rich conditions ($\Phi > 1$). The different steps of Φ were applied to ensure more precise analysis results due to the different sensitivity of system properties to Φ in different ranges, as shown in Table 1. For instance, a finer step of 0.05 was selected for $1.1 < \Phi < 1.7$ since the most complex trend between system response and Φ was observed in this range. The burner position was set as L/4, L/6, L/10 and L/12 from the bottom of the tube. The pressure fluctuations time series signal was measured by a pressure transducer microphone (PCB 377C10 and preamplifier PCB 426B03). The pressure-field microphone was placed at the bottom end and in the axial direction of the tube to ensure the pressure wave can incident in the perpendicular direction to the diaphragm and the temperature is not exceeding the upper limit of microphone operating temperature. The microphone unit utilised in this study has a linear response range from 10 Hz to 5000 Hz, which means the typical self-excited oscillation frequency in this study (around 180 Hz) is in the linear response ranges. The microphone was calibrated against a signal of 10 Pa at 1000 Hz before each experiment to ensure the accuracy of the result. The pressure signal with a length of at least 10 seconds was collected at a sampling rate of 100,000 Hz to provide a clear view of the recurrence plot and the accuracy of frequency analysis. NI-9205 Voltage input module with the Chassis cDAQ-9178 was utilised to collect the microphone signal. A stabilisation process of 3 minutes before recording was operated to ensure the stableness of the system and the system exit from the transition process.

2.2. Data processing and analysis

2.2.1. Phase difference

In order to analyse the relative positions between the components of different harmonic modes in the time domain, a FIR (Finite impulse response) filter was utilised to decompose the original time series signal to get the components of different harmonic modes. The 100,000 sample points (1 s) at the start and end of the filtered signal were cut to eliminate the unstable ranges. In this study, the fundamental harmonic mode was taken as the reference with no phase shift, shown as:

$$y_f = A\ \sin(t), \tag{1}$$

$$y_{n-th} = B\ \sin(n\ (t-\varphi)), \tag{2}$$

where y denotes the sinusoidal signal. The subscript f, n indicates the fundamental and n-th harmonic mode. φ is the phase difference to identify the relative position between two different harmonic modes in the oscillations. In this study, the phase difference calculation focused on the fundamental (y_f) and second (y_{2nd}) harmonic modes. The higher harmonic modes were ignored due to their neglectable intensity. If there is no phase difference between y_f and y_{2nd} ($\varphi = 0$), the relative 0 phase point of them will be the same. However, it is difficult to locate the relatively 0 phase point for the discrete time series. Therefore, the local maximum point (M) was used to determine the local phase difference for each period in this study.

A reference phase (φ_{ref}) is defined for the calculation of the local phase difference of each period, since the local maximum points of

Table 1
The step in different equivalence ratio ranges.

Equivalence ratio range	0.8 ~ 1.1	1.1 ~ 1.7	1.7 ~ 2.0	2.0 ~ 3.0	3.0 ~ 4.0	4.0 ~ 5.0
Step	0.1	0.05	0.1	0.2	0.25	0.5

y_f and y_{2nd} are at different positions due to the difference in frequency. The φ_{ref} is the time difference between the local maximum points of y_f and y_{2nd} when $\varphi = 0$. Note that the local maximum point of a sine wave is at the quarter of the period, the φ_{ref} can be then calculated based on the period of the y_f and y_{2nd}. The period for i-th oscillation can be obtained by the time difference between local maximum point at i and i + 1. Therefore, the local reference phase at α-th period of the fundamental mode (φ^{α}_{ref}) is:

$$\varphi^{\alpha}_{ref} = \frac{\left(M^{\alpha+1}_{f} - M^{\alpha}_{f}\right) - \left(M^{\beta+1}_{2} - M^{\beta}_{2}\right)}{4}, \tag{3}$$

where α, β denotes the α/β-th period of the fundamental/second harmonic mode. Note that the β-th period of the second harmonic mode is at the same time as the α-th period of the fundamental harmonic mode. The φ^{α}_{ref} calculated by Eq. (3) is in the unit of the sample point. Based on φ^{α}_{ref}, the local phase difference at α-th period of the fundamental mode ($\varphi^{\alpha}_{f,\,2}$) can be calculated as:

$$\varphi^{\alpha}_{f,\,2} = \frac{2\pi}{\left(M^{\beta+1}_{2} - M^{\beta}_{2}\right)}\left(\varphi^{\alpha}_{ref} - \left(M^{\alpha}_{f} - M^{\beta}_{2}\right)\right), \tag{4}$$

The mean phase difference ($\overline{\varphi_{f,2}}$) and the standard deviation (σ) are:

$$\overline{\varphi_{f,2}} = \frac{1}{k}\sum_{\alpha=1}^{k}\varphi^{\alpha}_{f,\,2}, \tag{5}$$

$$\sigma = \sqrt{\frac{1}{k}\sum_{\alpha=1}^{k}\left(\varphi^{\alpha}_{f,\,2} - \overline{\varphi_{f,2}}\right)^2}, \tag{6}$$

where k represents the k-th period of the fundamental mode. The σ was used to quantify the amount of variation for the local phase difference. The phase would be realigned if the $\varphi^{local}_{f,\,2}$ is greater than 2π, since the period of the second harmonic mode has the double value of the fundamental modes. A sample for the calculation of $\varphi^{local}_{f,2}$ can be provided as follows, as shown in Fig. 2. In this case, the local maximum points of α-th and α+1-th periods of fundamental harmonic mode are at 26391 and 26926, respectively. And 26393, 26660 for the local maximum points of β-th and β+1-th periods of second harmonic mode. Therefore, for α-th oscillation, the φ^{α}_{ref} can be calculated by Eq. (3) as:

$$\varphi^{\alpha}_{ref} = \frac{(26926 - 26391) - (26660 - 26393)}{4} = 67 \text{ points}, \tag{7}$$

According to Eq. (4), the $\varphi^{\alpha}_{f,\,2}$ is:

$$\varphi^{\alpha}_{f,\,2} = \frac{2\pi}{(26660 - 26393)}(67 - (26391 - 26393)) = 1.624 \text{ rad}, \tag{8}$$

2.2.2. Recurrence plot (RP) and recurrence quantification analysis (RQA)

The recurrence of the system state is an important characteristic for describing the system behaviour. Therefore, the recurrence analysis can effectively reveal the system dynamics properties of the nonlinear self-excited thermoacoustic oscillation. The RP enable the visualisation of recurrences and the identification of different states for a dynamical system from the phase space [35,46]. It has been utilised for analysing both external and self-excited thermoacoustic oscillation [23,33,42–44]. In this study, the space vector in the phase space was obtained based on Takens' time-delay embedding method [50]. For a discrete pressure fluctuation time series $p(t) \in \mathbb{R}$, the space vector x_t with an embedding dimension of D can be constructed from:

$$x_t(D) = (p(t), p(t-\tau), p(t-2\tau), \cdots, p(t-(D-1)\tau)), \tag{9}$$

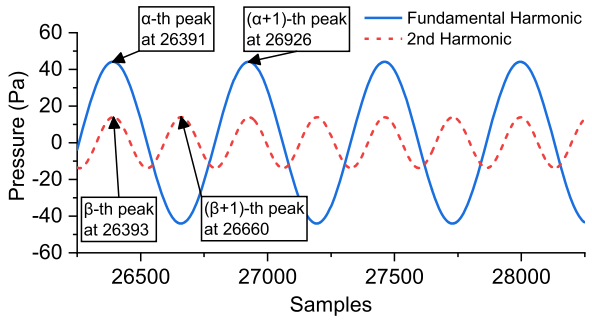

Fig. 2. Example of calculation for the local phase difference $\boldsymbol{\varphi^{local}_{f,2}}$.

where t denotes the time. τ is the time delay. It is suggested that the τ can be determined by autocorrelation function or average mutual information method [51]. In this study, τ was determined by the first zero-crossing point of the autocorrelation functions due to the low complexity of the periodic system. Besides, the D is crucial to the recurrence analysis as a proper D should avoid spurious correlations caused by the inappropriately high D, and the orthogonal diagonal lines to the line of identity (LOI, $R_{i,j} = 1$) caused by the inappropriately low D. In this study, D was set to 3 for all cases according to the results of the false nearest neighbour (FNN) method. Based on the $x_i(D)$, the binary recurrences matrix $R_{i,j}$ can be expressed in the following form:

$$R_{i,j} = \Theta\left(\varepsilon - \| x_i - x_j \|\right) \; i,j = 1,\ 2,\ 3,\ \cdots,\ N, \tag{10}$$

where ε denotes the threshold for recurrence plot computation, x_i and x_j are the space vectors and the subscripts i and j are the sequence number of space vectors. $\| x_i - x_j \|$ is the norm of the difference between x_i and x_j; Θ is the Heaviside function which has the definition as: $\Theta(x) = 0$, if $x\langle 0$; $\Theta(x) = 1$, if $x\rangle 0$; N is the number of points for recurrence analysis. According to Eq. (10), $R_{i,j}$ will be 0 if the $\| x_i - x_j \|$ exceeds ε, or 1 for those is smaller than ε. Based on the computation, a binary matrix R can be obtained. In this study, the black portion of the plot represents the $R_{i,j} = 1$, while the white portion for $R_{i,j} = 0$.

It has been found that a very high sampling rate can cause spurious quantifications and exclusively diagonal line structures in the RP if the system is highly periodic with a smooth phase space. As a result, the determinism (DET) can be too high to sufficiently show the characteristics of the periodic system [38,52]. Thus, a down-sampling process was performed to meet the suggested number of points for a period of 8 to 10 points [35].

Meanwhile, the threshold value ε is critical for obtaining a reasonable and reliable result. Schinkel et al. suggest that the ε should be no more than 10% of the mean phase space diameter [53]. In this study, ε was set as 15% of the standard deviation of the pressure fluctuation time series according to work conducted by Zan et al. [43]. Such value also satisfies the criterion proposed by Marwan [46].

In order to quantify the system dynamics from the RP, Recurrence Rate (RR), Determinism (DET), Shannon Entropy (ENT) and average diagonal line length (ADL) were obtained in this study. The corresponding equations are expressed below:

$$RR(\varepsilon) = \frac{1}{N^2}\sum_{i,j=1}^{N} R_{i,j}(\varepsilon), \tag{11}$$

$$DET = \frac{\sum_{l=l_{min}}^{N} lP(l)}{\sum_{l=1}^{N} lP(l)}, \tag{12}$$

$$ADL = \frac{\sum_{l=l_{min}}^{N} lP(l)}{\sum_{l=min}^{N} P(l)}, \tag{13}$$

$$ENT = -\sum_{l=l_{min}}^{N} p(l)\ln p(l), \tag{14}$$

where N represents the total length of the recurrence data, $P(l)$ is the histogram of the diagonal line with the length of l, and l_{min} is the predefined minimum length of the diagonal line. In this study, l_{min} is set to 2. $p(l)$ is the probability of the occurrence of the diagonal line with a length of l, which is calculated from $p(l) = P(l)/N_l$. N_l is the number of diagonal lines. The unit of ENT in this study is nat. For the RR, it can be used to measure the density of recurrence points based on the recurrence matrix $R_{i,j}$. Based on the diagonal structure in the plot, DET is defined as the ratio of the recurrence points that forms the diagonal lines to all recurrence points in R. Thus, DET is able to show the occurrence probability of similar states in the system. The ADL was used to indicate the degree of parallelism and the average time of two segments in the trajectory being close to each other [46]. Shannon information entropy was used to quantify the complexity of the system by obtaining the appearance probability of the diagonal lines with the length of exactly l in the plots.

3. Result and discussion

In this study, the self-excited thermoacoustic oscillation driven by a premixed methane-air laminar flame in a Rijke tube was investigated. The frequency response and oscillation amplitude (denoted by root mean square value of pressure) of the system were obtained at different methane flowrates, equivalence ratios and burner positions. An Φ-independence range and an Φ-dependence range were discovered under a given methane flowrate from the results. In detail, the system eigenfrequency trended to be independent with changing Φ. The time-domain analysis of phase difference, RP and RQA were processed for a further understanding of the characteristics of changes in time-evolution of pressure fluctuations ($p(t)$) and the system dynamics in Φ-independence. As a developed calculation method in this study, the phase difference was calculated to obtain the relative time difference between the fundamental and second harmonic modes. The phase difference and recurrence analysis results validate the existence of Φ-independence and Φ-dependence range. By comparing the systems with different Φ in the Φ-independence range at the same methane flowrate, similar characteristics from characteristics of changes in $p(t)$ and system dynamics between the systems can be discovered.

3.1. Determinations of Φ-dependence range and Φ-independence ranges

The eigenfrequency (f_{eigen}) and the root mean square value of pressure (P_{rms}) for the cases under different parameters are shown in Fig. 3. Considering the effects of system parameters on the system response, experiments at different burner positions and $\dot{m}_{CH_4}$ are conducted to verify the changing trends of f_{eigen}. The similar nonlinear trends between f_{eigen} and Φ can be observed in all cases regardless of system parameter changes. The f_{eigen} presents high sensitivity to the change of Φ in the range of approximately 1.1 to 2.2, and most cases show a decreasing trend, as shown in Fig. 3(a). However, as the Φ keeps increasing, the f_{eigen} trended to be stable and insensitive to the change of Φ. It can be also found that the f_{eigen} generally has a greater value in the Φ-dependence than in the Φ-independence range. According to the sensitivity of f_{eigen} to Φ, the range that the f_{eigen} presents high independence on Φ is defined as the Φ-independence range. Similarly, the Φ-dependence range is for the range that f_{eigen} is highly dependent on Φ. A criterion for determining the range can be raised based on the difference between corresponding f_{eigen} and the reference frequency in Φ-independence range ($\overline{f_{IR}}$). The $\overline{f_{IR}}$ is calculated from the mean f_{eigen} of all the cases with $\Phi \geq 3$, since it has been found that $\Phi = 3$ would be beyond the critical Φ ($\Phi_{critical}$) between the Φ-dependence and Φ-independence range. From the experimental results, it is found that the value of 0.5% in frequency difference between the f_{eigen} and $\overline{f_{IR}}$ is a proper criterion value for the critical Φ. It can be expressed as:

$$\frac{(f_{eigen} - \overline{f_{IR}})}{\overline{f_{IR}}} = \begin{cases} > 0.5\% \ \Phi - dependence\ range \\ \leq 0.5\% \ \Phi - independence\ range \end{cases}, \tag{15}$$

For instance, Fig. 4 shows the determination of the Φ-dependence and Φ-independence ranges for the cases at a burner position of L/4 and $\dot{m}_{CH_4} = 0.65$ L/min. From the typical flame photos shown in Fig. 5, it can be found that the flame length increases with the increasing Φ before the $\Phi_{critical}$, while becomes less varied with Φ once the Φ exceeds the $\Phi_{critical}$. Thus, the trend of flame length is also in good agreement with the Φ-dependence and Φ-independence range.

The $\Phi_{critical}$ and the relevant results of cases under different system parameters are shown in Table 2. The percentage difference between the f_{max} and $\overline{f_{IR}}$ validates the obvious eigenfrequency change as the Φ changes. Besides, the results of P_{rms} are presented in Fig. 3. A trend that the P_{rms} rapid increases in Φ-dependence range and then smoothly decreases in Φ-independence can be observed in the different cases regardless of changing system parameters. It is also found that the turning point of P_{rms} is located in Φ-dependence range. Thus, the oscillation amplitude of the system also conforms to the Φ-dependence and Φ-independence range determined based on the f_{eigen}.

3.2. Characterisation of Φ-dependence and Φ-independence ranges

The results of both f_{eigen} and P_{rms} show that the system presents a more sensitive response to the change of Φ in the Φ-dependence range than the Φ-independence range. From the time-evolution of the oscillation, it can be found that the amplitude of oscillation tends to be more fluctuated when the system is in the Φ-dependence range, as shown in Fig. 6. Besides, the case that the amplitude presents less time-variant characteristics tends to have simpler and 'cleaner' frequency spectrum compared to the cases that the amplitude is strongly varied with time, as shown in Fig. 6(c).

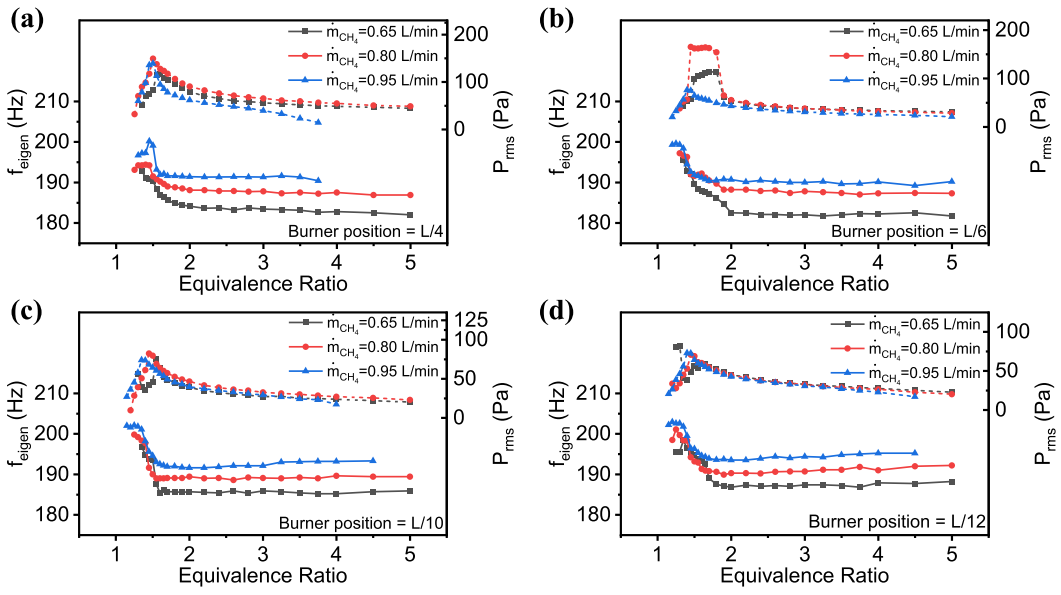

Fig. 3. f_{eigen} and P_{rms} to Φ diagram for the cases under different burner positions ((a) L/4, (b) L/6, (c) L/10 and (d) L/12) and $\dot{m}_{CH_4}$.

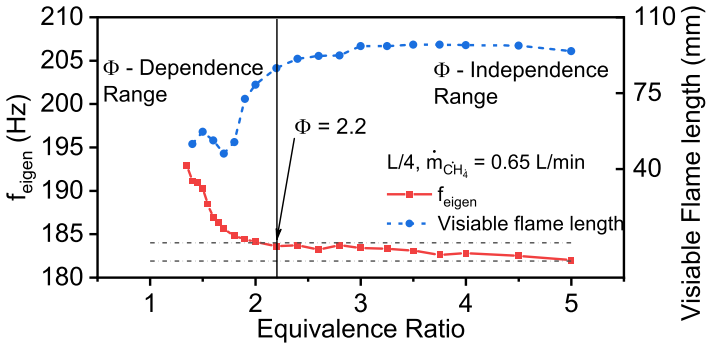

Fig. 4. Example of determination of the **Φ**-dependence and **Φ**-independence range for the case at L/4 of burner position and $\dot{m}_{CH_4} = 0.65\ L/min$. The red solid line represents the f_{eigen} and blue dashed line for the visible flame length. The critical **Φ** is at **Φ** = 2.2. The upper and the lower critical frequency for the range determination is 183.7 Hz and 181.9 Hz, respectively, shown in dashed-dot lines.

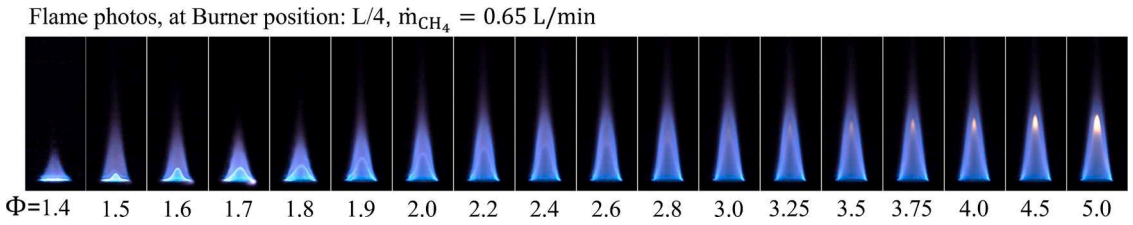

Fig. 5. Flame photos under different **Φ** for the case at burner position of L/4 and $\dot{m}_{CH_4}$=0.65 L/min.

Table 2
The relevant results of $\overline{f_{IR}}$, percentage difference between f_{max} and $\overline{f_{IR}}$ and the $\Phi_{critical}$ under different conditions.

Burner position	L/4			L/6			L/10			L/12		
$\dot{m}_{CH_4}$ (L/min)	0.65	0.8	0.95	0.65	0.8	0.95	0.65	0.8	0.95	0.65	0.8	0.95
$\overline{f_{IR}}$ (Hz)	182.8	187.2	191.2	182.1	188.3	190.8	185.6	189.2	192.6	187.5	191.1	194.7
$\frac{f_{max}-\overline{f_{IR}}}{\overline{f_{IR}}}$ (%)	5.55	4.27	4.71	7.32	5.23	4.97	6.03	5.60	4.88	5.81	5.23	4.21
$\Phi_{critical}$	2.2	2.0	1.7	2.0	1.9	1.65	1.6	1.5	1.5	1.8	1.6	1.6

An example case of L/12 in burner position and $\dot{m}_{CH_4}$ = 0.65 L/min is presented in Fig. 7(a) and (b). The standard deviation of the upper (σ_u) and lower (σ_l) envelop for the waveform in Φ-dependence range (Fig. 7(a), Φ = 1.45) are σ_u = 3.053 and σ_l = 1.857. Relatively, the corresponding values in Φ-independence range (Fig. 7(b), Φ = 4) are σ_u = 0.8044 and σ_l = 0.4161, which is much smaller than the case of Φ = 1.45. The difference in σ_u and σ_l indicate a larger variation of oscillation waveform envelope in Φ-dependence range than Φ-independence range. Besides, a clear shape in the waveform which indicates the period-2 oscillation can be observed in Fig. 7(a) and highlighted by green dashed line, while does not exist in Fig. 7(b). The shape in Fig. 7(a) indicates the notable intensity of the second harmonic mode. It needs to be noticed that the 2nd harmonic mode in the case of Φ = 4 still have an intensity that cannot be neglected, although it is less intense than the fundamental mode. By analysing the superposition of two sinusoidal signals with different frequencies, it is found that the relative position ('phase difference') between them in the time domain plays an important role in affecting the characteristics of changes in p(t). The phase difference and its variation with time can result in the variation of instantaneous oscillation amplitude and the shape of the time-series waveform. Therefore, the phase difference analysis is conducted to quantify the characteristics of changes in p(t) oscillation characteristics in both ranges.

3.3. Case analysis under different system parameters

Although the variations of f_{eigen} and time-evolution of pressure fluctuation show the existence of the Φ-dependence and Φ-independence range, it is necessary to further investigate the system behaviour in both ranges in terms of characteristics of changes in p(t) and system dynamics. Therefore, the phase difference analysis based on the FIR filter for the characteristics of changes in p(t) and both RP and RQA analysis for the system nonlinear dynamics are applied for further investigation in this study.

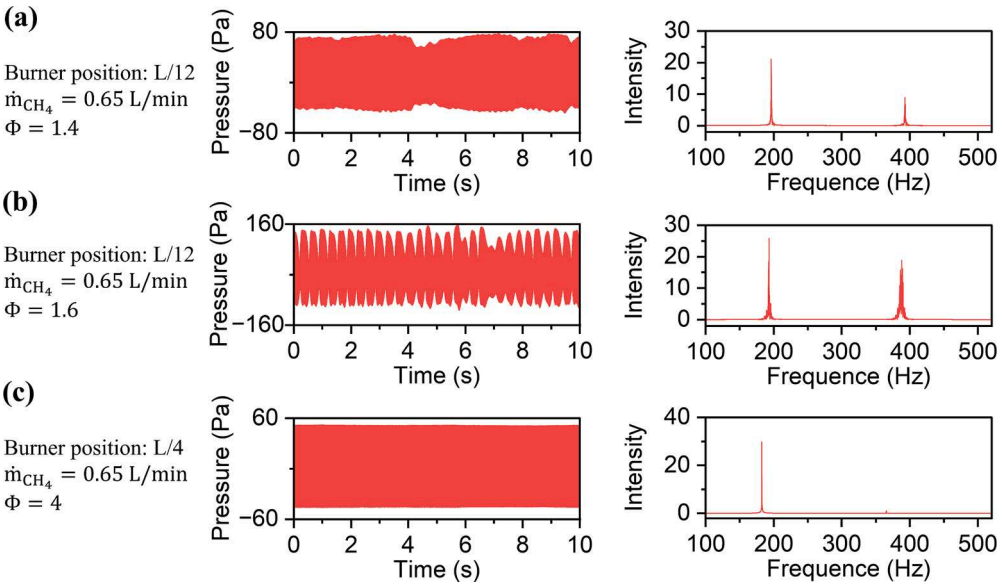

Fig. 6. The time-evolution of the pressure fluctuations (left) and the frequency spectrum (right) for the representative cases, (a) typical case in **Φ**-dependence range, (b) quasi-periodic oscillation (beating), (c) typical case in **Φ**-independence range. The experimental conditions are shown in the corresponding figures.

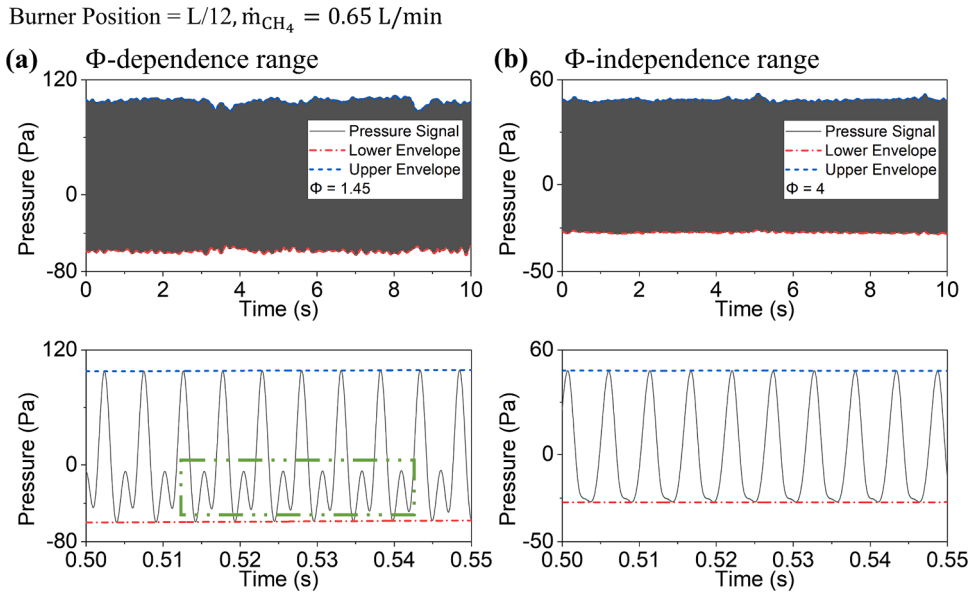

Fig. 7. Time-evolution of the pressure fluctuations for the cases of the burner at L/12, $\dot{m}_{CH_4}$ = 0.65 ***L/min***, (a) **Φ** = 1.45 and (b) **Φ** = 4. The diagram below them is their detailed zoom in time-evolution waveform. The green dash line highlights the difference in waveform between (a) period-2 oscillation to (b) period-1 oscillation. The blue and red lines represent the upper and lower envelope of the waveform, respectively.

3.3.1. Phase difference analysis (characteristics of changes in p(t)*)*

The results of the mean phase difference ($\overline{\varphi_{f,2}}$) and corresponding standard deviation σ with the changing Φ under different parameters are shown in Fig. 8. It can be found that the trend of both $\overline{\varphi_{f,2}}$ and σ conform to the determined Φ-dependence and Φ-independence range based on f_{eigen}. For the cases of L/12 in burner position and $\dot{m}_{CH_4}$ = 0.65 L/min, it is found that the $\overline{\varphi_{f,2}}$ trended to be stable and insensitive to the change of Φ when the Φ exceeds 1.8 while showing greater sensitivity before this Φ. Meanwhile, σ of $\varphi_{f,2}^{local}$ trends to be approximately 0 once the Φ becomes greater than 1.8, which indicates a very stable $\varphi_{f,2}^{local}$ during the oscillation. Under such circumstances, the system can be considered that has a lower complexity and approaches more stable limit-cycle oscillation in the Φ-independence range. By comparing the case with different $\dot{m}_{CH_4}$, from 0.65 to 0.95 L/min, it can be found that the trends of $\overline{\varphi_{f,2}}$ to Φ

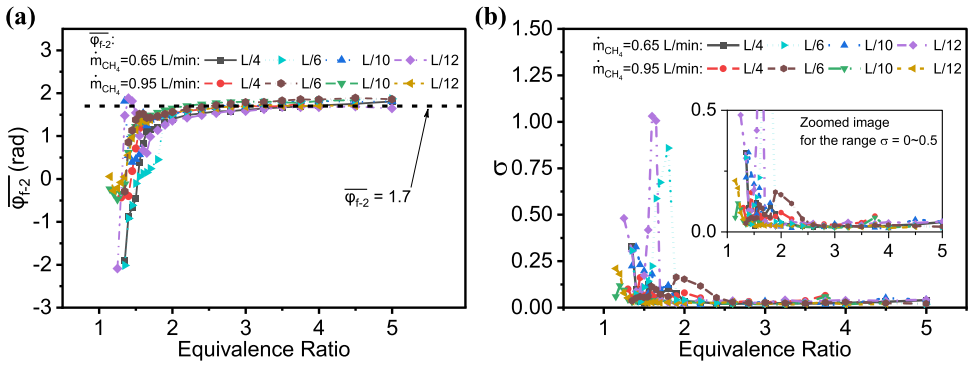

Fig. 8. Variation of (a) $\overline{\varphi_{f,2}}$, (b) $\boldsymbol{\sigma}$ to $\boldsymbol{\Phi}$. The colours represent the different case as shown in the legend.

is similar, but the $\overline{\varphi_{f,2}}$ of the case at $\dot{m}_{CH_4} = 0.95$ L/min is less varied with Φ when case is in Φ-independence range. By comparing the case at a higher burner position, from L/12 to L/10, no significant difference can be observed from the trends of $\overline{\varphi_{f,2}}$, but a larger difference in σ can be found as the burner moves downwards. Combining the results of the case at L/4 of the burner position, it is found that the trend of $\overline{\varphi_{f,2}}$ for all cases are similar, that both the $\overline{\varphi_{f,2}}$ and σ significantly changes if the system is in the Φ-dependence range and then gradually approaches constant value once it passes the $\Phi_{critical}$. Meanwhile, the changing rate of $\overline{\varphi_{f,2}}$ with increasing Φ becomes smaller once the Φ exceeds $\Phi_{critical}$, which indicates that the trend of $\overline{\varphi_{f,2}}$ is strong related to the Φ-dependence and Φ-independence range. The σ in Φ-dependence range are generally greater than those in the Φ-independence range, which further evidences a more stable and less complex system in the Φ-independence range. Besides, it is found that the value of σ is decreased along with the raising burner position and increasing $\dot{m}_{CH_4}$. Note that such results may indicate a more unstable oscillation at lower burner positions and lower $\dot{m}_{CH_4}$.

Then focusing on the case with the largest σ (purple line in Fig. 8(b), conditions as L/12, $\dot{m}_{CH4} = 0.65$ L/min and $\Phi = 1.6$), the corresponding frequency decomposing diagram and variation of $\varphi^{local}_{f,2}$ are shown in Fig. 9. From the original signal, it can be found that the beating oscillation is triggered in this case, and the system presents a quasi-periodic characteristic, as shown in Fig. 9(a). Meanwhile, it is found that the second harmonic mode dominates the beating oscillation rather than the fundamental mode, although the fundamental mode has a higher mean intensity, as shown in Fig. 6(b). From the diagram of the variation of $\varphi^{local}_{f,2}$, shown in Fig. 9(b), the presence of $\varphi^{local}_{f,2}$ frequently sudden phase shifting indicates an unstable system with a relatively high σ (about 1.03) and quasi-periodic characteristics. The result indicates the existence of frequency fluctuations during the self-excited oscillation when the beating oscillation is triggered.

Comparatively, the same diagrams for the case in the Φ-independence range at the same burner position and $\dot{m}_{CH_4}$ but a larger Φ of 3 is shown in Fig. 10. From both diagrams of frequency decomposing and $\varphi^{local}_{f,2}$, it can be observed that the $\varphi^{local}_{f,2}$ of the case in the Φ-independence range is more stable than the cases of $\Phi = 1.6$ which is in the Φ-dependence range. Since only slight variations of $\varphi^{local}_{f,2}$ with time ($\sigma = 0.023$) can be obtained, as shown in Fig. 10(b).

As an example of the oscillation without beating oscillation in the Φ-dependence range, Fig. 11(a) shows the time-evolution of the pressure fluctuations and the corresponding fundamental and second harmonic modes for the case of L/4, $\dot{m}_{CH4} = 0.65$ L /min, $\Phi = 1.35$. It can be found that the intensity of the second harmonic mode is lower than the fundamental mode. Due to the low intensity of the second harmonic mode, a similar waveform and phase between the fundamental mode and the original signal can be seen in Fig. 11(a). Although the frequency decomposing diagram shows a similar pattern to Fig. 10(a), the $\varphi^{local}_{f,2}$ in Fig. 11(b) presents a time-varied trend that is clearly decreasing trend with time. The unstable $\varphi^{local}_{f,2}$ and a greater σ of 0.326 indicate the oscillation is more complex and

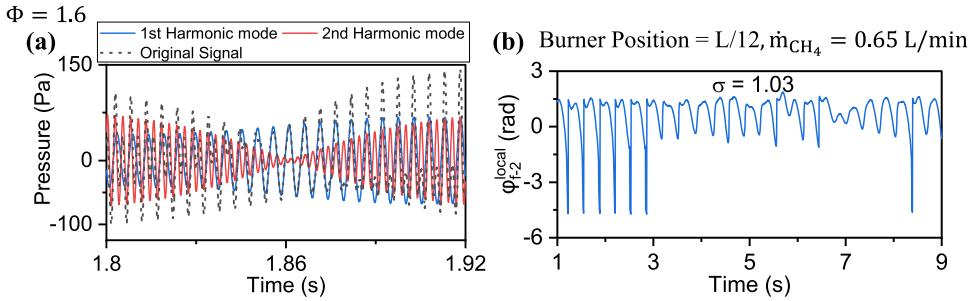

Fig. 9. (a) Frequency decomposing, and (b) $\boldsymbol{\varphi^{local}_{f,2}}$ diagram for the case L/12, $\boldsymbol{\dot{m}_{CH_4}} = 0.65$ ***L/min*** and $\boldsymbol{\Phi} = 1.6$. The case of the beating oscillation being triggered.

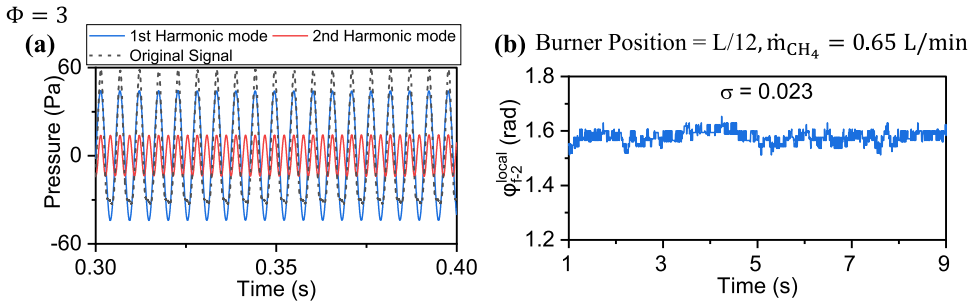

Fig. 10. (a) Frequency decomposing, and (b) $\boldsymbol{\varphi}_{f,2}^{local}$ diagram for the case L/12, $\dot{\boldsymbol{m}}_{\boldsymbol{CH_4}} = 0.65\ \boldsymbol{L/min}$ and $\boldsymbol{\Phi} = 3.0$. The case in **Φ**-independence range.

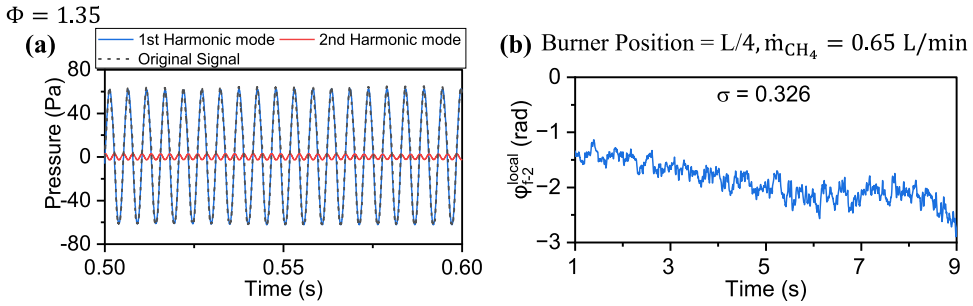

Fig. 11. (a) Frequency decomposing and (b) $\boldsymbol{\varphi}_{f,2}^{local}$ diagram for case L/4,$\dot{\boldsymbol{m}}_{\boldsymbol{CH_4}} = 0.65\ \boldsymbol{L/min}$, $\boldsymbol{\Phi} = 1.35$. The case in **Φ**-dependence range.

time-variant compared to the case L/12, $\dot{m}_{CH4} = 0.65$ L/min, and $\Phi = 3.0$.

In summary, it is found that both the trends of $\overline{\varphi_{f,2}}$ and the corresponding σ of $\varphi_{f,2}^{local}$ are strongly related to the characterisation of Φ-dependence and Φ-independence range. The similar value of $\Phi_{critical}$ for the trends of phase difference analysis and f_{eigen} can be found. Therefore, the Φ-dependence range and Φ-independence range can be also applicable for determining the dependency of characteristics of changes in p(t) on Φ. In detail, the $\overline{\varphi_{f,2}}$ is sensitive to the change of Φ in the Φ-dependence range but becomes less sensitive once the system enters the Φ-independence range. The σ in the Φ-dependence range is greater and presents greater variations than those in the Φ-independence range, indicating a more complex system in the Φ-dependence range. In addition, due to the greater sensitivity of phase difference to Φ, it can assist in the determination of both ranges. Besides, the $\overline{\varphi_{f,2}}$ in Φ-independence range shows less sensitivity to the change of burner position and $\dot{m}_{CH_4}$. It can be found that the values of $\overline{\varphi_{f,2}}$ under different burner positions and $\dot{m}_{CH_4}$ are similar in the Φ-independence range with approximate values ranging from 1.6~1.8 rad as the Φ increases. Considering the slight influence of $\dot{m}_{CH_4}$ on the phase difference as $\dot{m}_{CH_4}$ increases, the characteristics of changes in p(t) in the Φ-independence range might be strongly influenced by the acoustic properties of the resonance chamber.

Therefore, the trend of phase difference to varied Φ validates the existence of the Φ-dependence range and Φ-independence range. Since no significant phase difference changes in the Φ-independence range as the Φ changes can be observed. It can be considered that the characteristics of changes in p(t) conform to the range defined based on f_{eigen} and the system presents similar characteristics of changes in p(t) in the Φ-independence range under the same system parameters.

3.3.2. *Recurrence plot and RQA*

Recurrence analysis is applied to investigate system nonlinear dynamics in this study. Fig. 12 shows the RPs of the cases at a burner position of L/12 and $\dot{m}_{CH_4} = 0.65$ L/min. It can be found that most cases present uniformly distributed periodical patterns with clear continuous diagonal lines except the case at $\Phi = 1.6$ where the beating oscillation is triggered. The RP of the case at $\Phi = 1.25$ shows a great amount of scatter points rather than continuous diagonal lines, indicating the strong time-variant nature of the system. For the cases with relatively stable oscillation without significant change of the time-evolution of pressure fluctuations, a 'periodic' pattern without complex sub-structures can be observed, such as $\Phi = 1.35$, 2, 2.4 and 3, as shown in Fig. 12(b) (d) (e) and (f). The clear continuous diagonal lines indicate that the system is highly periodic and quasi-stable [23,35,42,45]. For the case with more periodic natures ($\Phi = 1.35$, 2, 2.4 and 3), the diagonal lines tend to be more gathered, and fewer scatter points can be found compared to the case with higher complexity ($\Phi = 1.25$). Besides, although the density of diagonal lines seems to be higher for the case of $\Phi = 1.35$, the diagonal lines are more frequently interrupted and more scatter points can be found in the plot compared to the case in the Φ-independence range ($\Phi = 2$, 2.4 and 3). Therefore, it can be considered that the cases in the Φ-independence range have more periodic natures and is more stable than the cases in the Φ-dependence range without quasi-periodic characteristics.

For the case at $\Phi = 1.6$ with quasi-periodic characteristics, a frequently pattern change with 'high density' and 'low density' areas can be clearly observed (Fig. 12(c)), indicating the unstable system with state changes. The 'high density' area indicates the relatively

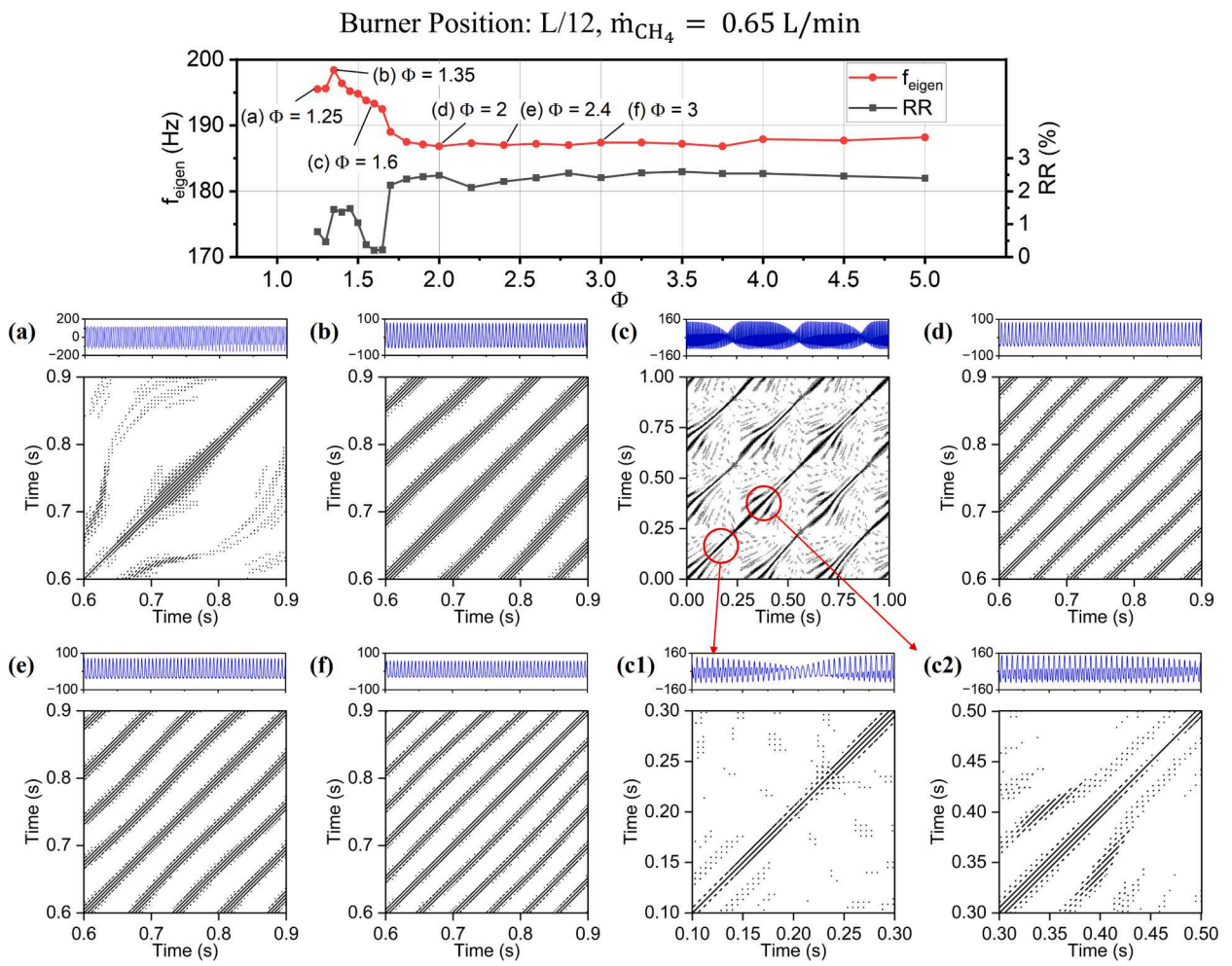

Fig. 12. Recurrence plots at (a) $\boldsymbol{\Phi} = 1.25$, (b) $\boldsymbol{\Phi} = 1.35$, (c) $\boldsymbol{\Phi} = 1.6$, (d) $\boldsymbol{\Phi} = 2$, (e) $\boldsymbol{\Phi} = 2.4$ and (f) $\boldsymbol{\Phi} = 3$ and the $\boldsymbol{f_{eigen}}$ and RR to $\boldsymbol{\Phi}$ diagram for case L/12, $\boldsymbol{\dot{m}_{CH_4}} = 0.65\ \boldsymbol{L/min}$. (c1): Zoomed RP of (c) at the low density area (beating range). (c2): Zoomed RP of (c) at the high density area. D = 3, $\boldsymbol{\tau}$ is determined by first zero-crossing point of the corresponding autocorrelation function.

stable oscillation (Fig. 10(c2)), whereas the 'low density' area (Fig. 10(c1)) represents where the beating happens. From Fig. 12(c), the bowed structure can be observed, which indicates the evolution of states has similarities but with different changing rates (the change of the frequency in this case), and the dynamic of the system is changing with time [46]. Meanwhile, no clear continuous diagonal lines can be observed apart from the LOI, which evidences the system state is strongly interrupted and the state transition frequently happens. From Fig. 12(c1), it can be found that the plot of 'low density' area (beating region) mainly consists of scatter points, and diagonal lines exist only next to the LOI. As the system exits the beating region, more recurrence points start to appear, and several diagonal lines start to be generated by the relatively stable oscillation, as shown in Fig. 12(c2) ('high density' area). The presence of the pattern 'density' change also evidences the existence of multiple states in a quasi-periodic system.

By comparing the curve of f_{eigen} and RR, it can be found that the range of RR and f_{eigen} presenting great sensitivities to the change of Φ is coincident with each other. A higher RR results from more recurrence points in the plot, indicating that the system dynamics can be also in agreement with the Φ-dependence and Φ-independence range.

To further quantify the system nonlinear dynamical properties, RR, DET, ENT and ADL are calculated based on the structural characteristics in the corresponding RP. The RR and DET are used to indicate the system recursiveness and occurrence of similar states for the thermoacoustic oscillation, respectively. The ENT can provide a quantitative measure of the system chaoticity. The ADL can indicate the divergence of the two segments in the phase space trajectory [44,46]. The results of these measures are shown in Fig. 13.

The RQA results are generally in agreement with the findings from the analysis of RP. Focusing on the same cases at a burner position of L/12 and $\dot{m}_{CH_4} = 0.65$ L/min, it is observed from Fig. 12 that the cases in the Φ-independence range ($\Phi = 2$, 2.4 and 3) have greater densities of recurrence points than the case in the Φ-dependence range ($\Phi = 1.25$, 1.35 and 1.6). The higher density of recurrence points results in a greater RR for the cases in the Φ-independence range. Meanwhile, the systems in the Φ-independence range have similar patterns of parallel and continuous diagonal lines, but the distinguishable difference in pattern for the systems in the Φ-dependence range. Therefore, the values of RR for the system in the Φ-independence range are similar and insensitive to the change

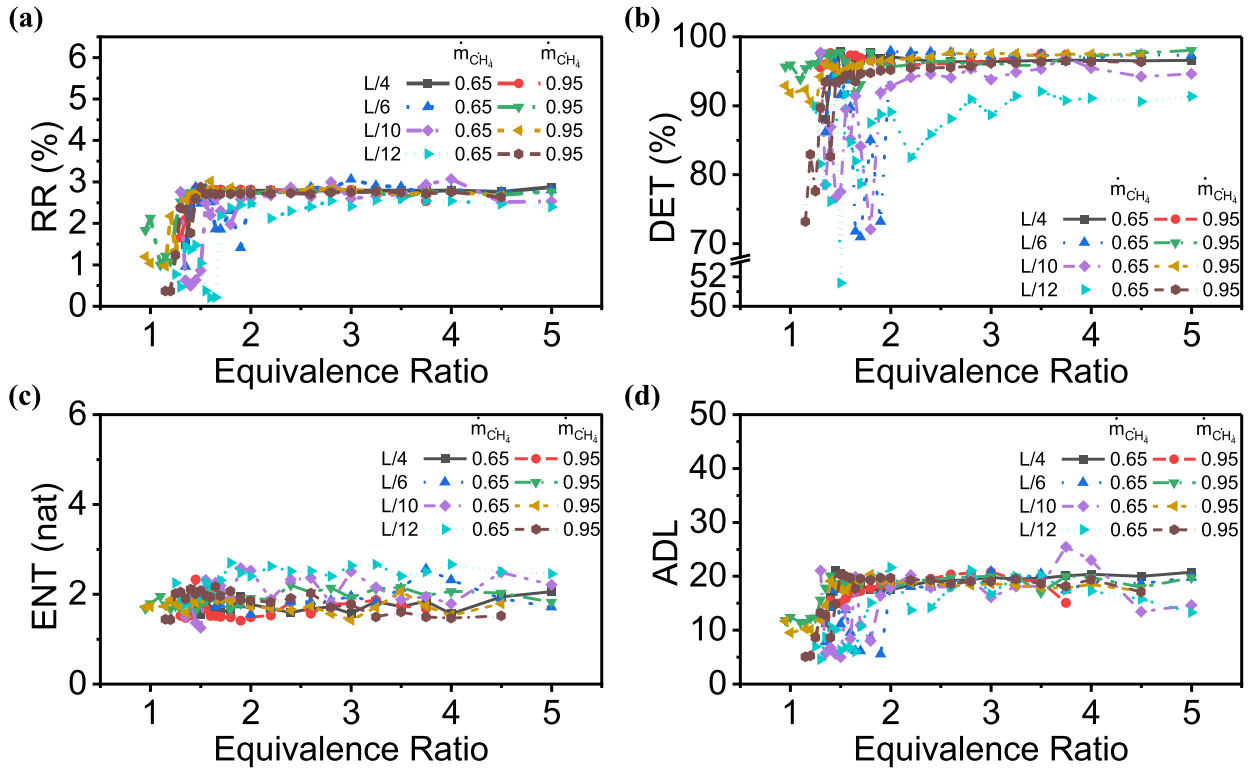

Fig. 13. Variation of four measures of RQA as the equivalence ratio changes. These four figures represent the: (a) recurrence rate, (b) determinism, (c) Shannon entropy, and (d) average diagonal length. The different curves with different colours represent the case with different burner positions or methane flowrate.

of Φ, but strongly vary with Φ if the system is in the Φ-dependence range, as shown in Fig. 13(a).

From the structural properties of the pattern, the longer diagonal lines with fewer interruptions can be observed from the RP of the system in the Φ-independence range, and the RP is mainly composed of diagonal lines as the less amount of scatter points exists, as shown in Fig. 12(d) ~ (f). In contrast, the RP of the system in the Φ-dependence range has short and less diagonal structures and the RP mainly consists of scatter points and very short diagonal line fragments, as shown in Fig. 12(a) ~ (c). The difference in the amount of diagonal lines results in the lower DET and ADL for the system in the Φ-dependence range. It can be found that the value of DET for most systems in the Φ-independence range is generally greater than 90%. However, for the systems in the Φ-dependence range, a clear lower DET that mostly ranges from 51% to 90% can be obtained, as shown in Fig. 13(b). Furthermore, the DET and ADL show a high dependence on Φ in the Φ-dependence range due to the considerable pattern change but low dependence in the Φ-independence range caused by similar patterns.

Different from the RR, DET and ADL, the ENT presents a low sensitivity to the change of Φ in both the Φ-dependence and Φ-independence range, and the values of ENT are relatively small, even for the system with quasi-periodic characteristics ($\Phi = 1.6$). The low sensitivity and the small value of ENT are caused by the considerable periodicity of the system and the neglectable chaoticity, since neither intermittency nor the chaotic state is found in this study.

By comparing the systems at different burner positions and $\dot{m}_{CH_4}$, the same findings can be drawn that the RR, DET and ADL present great sensitivities to the change of Φ in the Φ-dependence range but insensitivity in the Φ-independence range, as shown in Fig. 13. Meanwhile, the ENT shows less dependence on Φ in both ranges. It can be found that the higher RR and DET in the Φ-independence range can be obtained for all the cases, indicating a more stable system with less time-variant characteristics and a higher occurrence probability of similar states in the Φ-independence range, as shown in Fig. 13(a) (b). The lower ADL in the Φ-dependence range indicates that the two segments in the phase space trajectory tend to diverge faster and have lower degrees of parallelism in the phase space [44]. The result of ADL further evidences the more time-variant characteristics for the system in the Φ-dependence range. Besides, the results of ENT indicate that the systems in this study are generally periodic without noticeable chaoticity.

In summary, the RR, DET and ADL present different sensitivity as the Φ changes, which proves that the change of the system dynamics is also in agreement with the Φ-dependence and Φ-independence range. Thus, the existence of both ranges can be highlighted from the system dynamics. Meanwhile, the independence of ENT on Φ shows that the chaoticity of the system is less influenced by the Φ if the self-excited limit-cycle or quasi-periodic oscillation is triggered.

4. Conclusions

In this study, the effect of equivalence ratio (Φ) on the self-excited thermoacoustic oscillation in a Rijke tube was experimentally investigated. The changes in the frequency response and oscillation amplitude with the changing Φ were obtained and verified at varied burner positions and methane flowrate. Based on the pressure fluctuations time series, multiple time-domain data analysis methods were utilised to reveal the characteristics of system nonlinearity qualitatively and quantitatively. Specifically, the phase difference analysis successfully indicates the characteristics of changes in time-evolution of pressure fluctuations ($p(t)$) by obtaining the relationship between the fundamental and second harmonic modes in terms of time. The recurrence analysis effectively and directly provides the system dynamics characteristics by analysing and quantifying the structural properties of the recurrence plot (RP).

From the experimental results, it has been found that the self-excited thermoacoustic oscillation at different burner positions and methane flowrates can be strongly affected by Φ under the fuel-rich condition. A nonlinear trend of system frequency response to Φ was discovered. Based on the dependence of oscillation eigenfrequency on Φ, a Φ-dependence range that the eigenfrequency (f_{eigen}) presented strong dependence on Φ, and a Φ-independence range that the f_{eigen} was insensitive to the change of Φ were obtained. The results of phase difference and recurrence analysis were in good agreement with the nonlinear trend of f_{eigen}. The good agreement indicated that the sensitivity of characteristics of changes in $p(t)$ and system dynamics to Φ also conformed to the Φ-dependence and Φ-independence range. Besides, the results of phase difference analysis showed that the local phase difference in the Φ-independence range had less time-variant characteristics with a lower value of standard deviation. It indicates a more stable oscillation in the Φ-independence range. Meanwhile, a more stable and less time-varied system was also evidenced by the results of the recurrence analysis. From the results of system dynamics via RP and RQA, it was found that the system in the Φ-independence range tended to have a higher periodicity and lower complexity. While the chaoticity can be neglected for the periodic and quasi-periodic system in this study. The sensitivity of characteristics of changes in $p(t)$ and system dynamics validated the existence of both ranges and highlighted the importance of Φ in influencing the self-excited thermoacoustic oscillations. As a meaningful yet interesting finding, the mechanism of similar mean phase difference in the Φ-independence range, regardless of system parameter changes, should be carried out in future work. Meanwhile, considering the effects of system parameters on both frequency response and system dynamics, further study is worthy of being continued.

This study shows the critical role of Φ on self-excited oscillation in a Rijke tube. In this study, a developed phase difference calculation was applied to observe the characteristics of thermoacoustic oscillation. It is found that the analysis of phase difference can effectively indicate characteristics of changes in $p(t)$ and detect the exact time point where the oscillation behaviour changes. The methods utilised in this study are applicable to difference combustion system with nonlinearities. However, the filter for frequency decomposition in this study is challenging to be applied in analysing instantaneous system response. Also, the phase difference analysis is difficult to be achieved for the combustion with indirect combustion noise (noise of uniformly distributed intensity in the frequency domain). The future work for overcoming such shortages will be carried on.

CRediT authorship contribution statement

Xuanqi Liu: Conceptualization, Methodology, Software, Formal analysis, Investigation, Writing – original draft, Visualization. **Hangxu Zhou:** Validation, Writing – review & editing, Formal analysis. **Yufeng Lai:** Resources, Writing – review & editing, Investigation. **Yang Zhang:** Supervision.

Declaration of Competing Interest

The authors declare that they have no known competing financial interests or personal relationships that could have appeared to influence the work reported in this paper.

Data availability

Data will be made available on request.

Acknowledgements

This study has received no external funding.

References

[1] A.P. Dowling, The calculation of thermoacoustic oscillations, J. Sound Vib. 180 (1995) 557–581, https://doi.org/10.1006/JSVI.1995.0100.
[2] T.C. Lieuwen, Unsteady Combustor Physics, Cambridge University Press, Cambridge, 2012, https://doi.org/10.1017/CBO9781139059961.
[3] R.I. Sujith, S.A. Pawar, Thermoacoustic Instability, Springer International Publishing, Cham, 2021, https://doi.org/10.1007/978-3-030-81135-8.
[4] Rayleigh, The explanation of certain acoustical phenomena 1, Nature 18 (1878) 319–321, https://doi.org/10.1038/018319a0.
[5] M.P. Juniper, R.I. Sujith, Sensitivity and nonlinearity of thermoacoustic oscillations, Annu. Rev. Fluid Mech. 50 (2018) 661–689, https://doi.org/10.1146/annurev-fluid-122316-045125.

[6] F.E.C. Culick, Short communication a note on Rayleigh's criterion, Combust. Sci. Technol. 56 (1987) 159–166, https://doi.org/10.1080/00102208708947087.
[7] F. Nicoud, T. Poinsot, Thermoacoustic instabilities: should the Rayleigh criterion be extended to include entropy changes? Combust. Flame 142 (2005) 153–159, https://doi.org/10.1016/j.combustflame.2005.02.013.
[8] L. Magri, M.P. Juniper, J.P. Moeck, Sensitivity of the Rayleigh criterion in thermoacoustics, J. Fluid Mech. 882 (2020) R1, https://doi.org/10.1017/jfm.2019.860.
[9] A.A. Putnam, W.R. Dennis, Burner oscillations of the gauze-tone type, J. Acoust. Soc. Am. 26 (1954) 716–725, https://doi.org/10.1121/1.1907406.
[10] K. Balasubramanian, R.I. Sujith, Thermoacoustic instability in a Rijke tube: non-normality and nonlinearity, Phys. Fluids 20 (2008), 044103, https://doi.org/10.1063/1.2895634.
[11] D. Zhao, Z.H. Chow, Thermoacoustic instability of a laminar premixed flame in Rijke tube with a hydrodynamic region, J. Sound Vib. 332 (2013) 3419–3437, https://doi.org/10.1016/j.jsv.2013.01.031.
[12] P. Chatterjee, U. Vandsburger, W.R. Saunders, V.K. Khanna, W.T. Baumann, On the spectral characteristics of a self-excited Rijke tube combustor - numerical simulation and experimental measurements, J. Sound Vib. 283 (2005) 573–588, https://doi.org/10.1016/j.jsv.2004.04.019.
[13] K.I. Matveev, Energy consideration of the nonlinear effects in a Rijke tube, J. Fluids Struct. 18 (2003) 783–794, https://doi.org/10.1016/j.jfluidstructs.2003.07.016.
[14] J.A. Carvalho, M.A. Ferreira, C. Bressan, J.L.G. Ferreira, Definition of heater location to drive maximum amplitude acoustic oscillations in a Rijke tube, Combust. Flame 76 (1989) 17–27, https://doi.org/10.1016/0010-2180(89)90073-4.
[15] N.N. Deshmukh, S.D. Sharma, Suppression of thermo-acoustic instability using air injection in horizontal Rijke tube, J. Energy Inst. 90 (2017) 485–495, https://doi.org/10.1016/j.joei.2016.03.001.
[16] F. Weng, S. Li, D. Zhong, M. Zhu, Investigation of self-sustained beating oscillations in a Rijke burner, Combust. Flame 166 (2016) 181–191, https://doi.org/10.1016/j.combustflame.2016.01.016.
[17] U. Sen, T. Gangopadhyay, C. Bhattacharya, A. Mukhopadhyay, S. Sen, Dynamic characterization of a ducted inverse diffusion flame using recurrence analysis, Combust. Sci. Technol. 190 (2018) 32–56, https://doi.org/10.1080/00102202.2017.1374952.
[18] X. Wu, M. Wang, P. Moin, N. Peters, Combustion instability due to the nonlinear interaction between sound and flame, J. Fluid Mech. 497 (2003), S0022112003006554, https://doi.org/10.1017/S0022112003006554.
[19] M.A. Heckl, M.S. Howe, Stability analysis of the Rijke tube with a Green's function approach, J. Sound Vib. 305 (2007) 672–688, https://doi.org/10.1016/j.jsv.2007.04.027.
[20] Y. Guan, V. Gupta, L.K.B. Li, Intermittency route to self-excited chaotic thermoacoustic oscillations, J. Fluid Mech. 894 (2020) R3, https://doi.org/10.1017/jfm.2020.297.
[21] B. Zhang, M. Shahsavari, Z. Rao, S. Yang, B. Wang, Thermoacoustic instability drivers and mode transitions in a lean premixed methane-air combustor at various swirl intensities, Proc. Combust. Inst. 38 (2021) 6115–6124, https://doi.org/10.1016/j.proci.2020.06.226.
[22] J. Moeck, M. Bothien, S. Schimek, A. Lacarelle, C. Paschereit, Subcritical thermoacoustic instabilities in a premixed combustor, in: Proceedings of the 14th AIAA/CEAS Aeroacoustics Conference (29th AIAA Aeroacoustics Conference), American Institute of Aeronautics and Astronautics, Reston, Virigina, 2008, https://doi.org/10.2514/6.2008-2946.
[23] H. Zhao, G. Li, D. Zhao, Z. Zhang, D. Sun, W. Yang, S. Li, Z. Lu, Y. Zheng, Experimental study of equivalence ratio and fuel flow rate effects on nonlinear thermoacoustic instability in a swirl combustor, Appl. Energy 208 (2017) 123–131, https://doi.org/10.1016/j.apenergy.2017.10.061.
[24] S. Tachibana, K. Saito, T. Yamamoto, M. Makida, T. Kitano, R. Kurose, Experimental and numerical investigation of thermo-acoustic instability in a liquid-fuel aero-engine combustor at elevated pressure: validity of large-eddy simulation of spray combustion, Combust. Flame 162 (2015) 2621–2637, https://doi.org/10.1016/j.combustflame.2015.03.014.
[25] D. Zhao, Y. Chew, Energy harvesting from a convection-driven Rijke-Zhao thermoacoustic engine, J. Appl. Phys. 112 (2012), 114507, https://doi.org/10.1063/1.4767914.
[26] Y. Sun, D. Zhao, C. Ji, T. Zhu, Z. Rao, B. Wang, Large-eddy simulations of self-excited thermoacoustic instability in a premixed swirling combustor with an outlet nozzle, Phys. Fluids 34 (2022), 044112, https://doi.org/10.1063/5.0087055.
[27] S. Li, D. Zhao, C. Ji, J. Li, Combustion instabilities in a bifurcating tube: open- and closed-loop measurements, AIAA J. 52 (2014) 2513–2523, https://doi.org/10.2514/1.J052758.
[28] X. Song, T. Zhu, D. Pan, Z. Wang, C. Ji, D. Zhao, Numerical investigations on the beating behavior of self-excited combustion instability in a hydrogen-fueled Rijke type combustor, Aerosp. Sci. Technol. 126 (2022), 107624, https://doi.org/10.1016/j.ast.2022.107624.
[29] C.O. Paschereit, W. Polifke, Investigation of the thermoacoustic characteristics of a lean premixed gas turbine burner. Volume 3: Coal, Biomass and Alternative Fuels; Combustion and Fuels; Oil and Gas Applications; Cycle Innovations, American Society of Mechanical Engineers, 1998, https://doi.org/10.1115/98-GT-582.
[30] S. Mariappan, R.I. Sujith, P.J. Schmid, Experimental investigation of non-normality of thermoacoustic interaction in an electrically heated Rijke tube, Int. J. Spray Combust. Dyn. 7 (2015) 315–352, https://doi.org/10.1260/1756-8277.7.4.315.
[31] D. Zhao, A real-time plane-wave decomposition algorithm for characterizing perforated liners damping at multiple mode frequencies, J. Acoust. Soc. Am. 129 (2011) 1184–1192, https://doi.org/10.1121/1.3533724.
[32] Y. Sun, Z. Rao, D. Zhao, B. Wang, D. Sun, X. Sun, Characterizing nonlinear dynamic features of self-sustained thermoacoustic oscillations in a premixed swirling combustor, Appl. Energy 264 (2020), 114698, https://doi.org/10.1016/j.apenergy.2020.114698.
[33] Y. Guan, V. Gupta, L.K.B. Li, Intermittency route to self-excited chaotic thermoacoustic oscillations, J. Fluid Mech. 894 (2020), https://doi.org/10.1017/jfm.2020.297.
[34] S. Tandon, R.I. Sujith, Condensation in the phase space and network topology during transition from chaos to order in turbulent thermoacoustic systems, Chaos Interdiscip. J. Nonlinear Sci. 31 (2021), 043126, https://doi.org/10.1063/5.0039229.
[35] V. Nair, R.I. Sujith, Intermittency as a transition state in combustor dynamics: an explanation for flame dynamics near lean blowout, Combust. Sci. Technol. 187 (2015) 1821–1835, https://doi.org/10.1080/00102202.2015.1066339.
[36] L. Kabiraj, R.I. Sujith, Nonlinear self-excited thermoacoustic oscillations: intermittency and flame blowout, J. Fluid Mech. 713 (2012) 376–397, https://doi.org/10.1017/jfm.2012.463.
[37] A. Seshadri, V. Nair, R.I. Sujith, A reduced-order deterministic model describing an intermittency route to combustion instability, Combust. Theor. Model. 20 (2016) 441–456, https://doi.org/10.1080/13647830.2016.1143123.
[38] T. Braun, V.R. Unni, R.I. Sujith, J. Kurths, N. Marwan, Detection of dynamical regime transitions with lacunarity as a multiscale recurrence quantification measure, Nonlinear Dyn. 104 (2021) 3955–3973, https://doi.org/10.1007/s11071-021-06457-5.
[39] H. Gotoda, Y. Shinoda, M. Kobayashi, Y. Okuno, S. Tachibana, Detection and control of combustion instability based on the concept of dynamical system theory, Phys. Rev. E 89 (2014), 022910, https://doi.org/10.1103/PhysRevE.89.022910.
[40] Y. Shinchi, N. Takeda, H. Gotoda, T. Shoji, S. Yoshida, Early detection of thermoacoustic combustion oscillations in staged multisector combustor, AIAA J. 59 (2021) 4086–4093, https://doi.org/10.2514/1.J060268.
[41] H. Gotoda, Y. Okuno, K. Hayashi, S. Tachibana, Characterization of degeneration process in combustion instability based on dynamical systems theory, Phys. Rev. E 92 (2015), 052906, https://doi.org/10.1103/PhysRevE.92.052906.
[42] C. Tao, H. Zhou, Effects of operating parameters on the combustion oscillation behaviour in a lean premixed CH4 combustor, J. Mech. Sci. Technol. 35 (2021) 3753–3762, https://doi.org/10.1007/s12206-021-0744-4.
[43] H. Zan, W. Zhou, X. Xiao, L. Lin, J. Zhang, H. Li, Recurrence network analysis for uncovering dynamic transition of thermo-acoustic instability of supercritical hydrocarbon fuel flow, Aerosp. Sci. Technol. 85 (2019) 1–12, https://doi.org/10.1016/j.ast.2018.11.040.
[44] M. Murugesan, S. Balusamy, S. Hochgreb, L.K.B. Li, Recurrence analysis of forced synchronization in a self-excited thermoacoustic system, in: Proceedings of the 24th International Congress on Sound and Vibration, ICSV, 2017, https://doi.org/10.17863/CAM.33084.

[45] L.-P. Yang, S.-L. Ding, G. Litak, E.-Z. Song, X.-Z. Ma, Identification and quantification analysis of nonlinear dynamics properties of combustion instability in a diesel engine, Chao Interdiscip. J. Nonlinear Sci. 25 (2015), 013105, https://doi.org/10.1063/1.4899056.
[46] N. Marwan, M. Carmenromano, M. Thiel, J. Kurths, Recurrence plots for the analysis of complex systems, Phys. Rep. 438 (2007) 237–329, https://doi.org/10.1016/j.physrep.2006.11.001.
[47] K.T. Kim, Nonlinear interactions between the fundamental and higher harmonics of self-excited combustion instabilities, Combust. Sci. Technol. 189 (2017) 1091–1106, https://doi.org/10.1080/00102202.2016.1275591.
[48] G.S. Samuelsen, J. Brouwer, M.A. Vardakas, J.D. Holdeman, Experimental and modeling investigation of the effect of air preheat on the formation of NOx in an RQL combustor, Heat Mass Transf. 49 (2013) 219–231, https://doi.org/10.1007/s00231-012-1080-0.
[49] M. Khosravy, Review of the new combustion technologies in modern gas turbines. Progress in Gas Turbine Performance, InTech, 2013, https://doi.org/10.5772/54403.
[50] F. Takens, Detecting strange attractors in turbulence, in: 1981: pp. 366–381. 10.1007/BFb0091924.
[51] H. Gotoda, H. Nikimoto, T. Miyano, S. Tachibana, Dynamic properties of combustion instability in a lean premixed gas-turbine combustor, Chaos Interdiscip. J. Nonlinear Sci. 21 (2011), 013124, https://doi.org/10.1063/1.3563577.
[52] N. Marwan, How to avoid potential pitfalls in recurrence plot based data analysis, Int. J. Bifurcation Chaos 21 (2011) 1003–1017, https://doi.org/10.1142/S0218127411029008.
[53] S. Schinkel, O. Dimigen, N. Marwan, Selection of recurrence threshold for signal detection, Eur. Phys. J. Spec. Top. 164 (2008) 45–53, https://doi.org/10.1140/epjst/e2008-00833-5.